JOURNAL OF MECHANICS OF CONTINUA AND MATHEMATICAL SCIENCES
www.journalimcms.org

ISSN (Online) : 2454 -7190 Vol.-17, No.-5, May (2022) pp 1-15 ISSN (Print) 0973-8975

TURBULENT FLOW CHARACTERISTICS OF DUAL JET INTERACTIONS USING DIFFERENT TURBULENCE MODELS

Bouaraour Kamel[1], Lalmi Djemoui[2]

[1] Professor, Laboratory of Materials, Energetic Systems Technology and Environment. University of Ghardaia, Ghardaia, Algeria.

[2] Professor, Laboratory of Materials, Energetic Systems Technology and Environment. University of Ghardaia, Ghardaia, Algeria.

Email: [1] bouaraourk@yahoo.fr, [2] eldjemoui@gmail.com

Corresponding Author: **Bouaraour Kamel**

Email: bouaraourk@yahoo.fr

https://doi.org/10.26782/jmcms.2022.05.00001

Abstract

This paper, reports the numerical results of the turbulent flow characteristics and turbulent quantities when a triangular object is placed at the exit of two nozzles. The fluid flow at the entrance of the nozzles is considered isothermal and incompressible. Three turbulence k-ε models are used to study the jets interaction and its resulting characteristics. The numerical method is first validated with the available experimental results for a configuration where no object is placed between nozzles. Numerical simulations are carried out for fixed turbulence intensity at the nozzles exit (3%), and for Reynolds numbers varied from 2.10^3 to 10^4. Results reveal that the existence of a solid object between the dual jets affects the location of the merge and combined points. The merge point is pushed downstream of the flow, and the corresponding axial velocity of the combined point is reduced for all Reynolds numbers. The turbulent kinetic energy field is also affected, either in the near field or in the far field for all Reynolds numbers. We have concluded also that the Realizable k-ε model overestimates velocity and turbulent kinetic energy fields compared to the other models.

Keywords: flow interaction, merge point, combined point, turbulence model.

I. Introduction

Two jets interactions are encountered in many practical engineering applications such as injection systems, burners, mixing, and drying processes. The interaction between the two jets passes throw many steps until it merges into a single flow. The existence of three distinguished regions in the twin parallel jets configuration has been predicted first by Tanaka [XXIV, XXIII]. The converging region is located between the nozzles exit and the point where the shear layers of the jets merge. The transition region begins from the merging point to the combined point. The combined region starts where the two jets begin to resemble a self-similar single jet. Many years

later, Elbanna et al [VI] showed that the mean velocity profile of the parallel jets is similar to that of the single jet in the region downstream of the combined point. Through an experimental study, where hot-wire anemometry is used, Lin and Sheu [XIII, XII] discover that the velocity field approaches self-preservation either in the merging zone or in the combined zone.

An experimental study is carried out to investigate the interactions created by two air jets issuing from two identical plane inclined nozzles using a hot wire anemometer [XXVI]. The reverse flow has been detected by using the split film probe and observed by flow visualization. Experimental results with an inclined angle of 9° were presented. Results with an inclined angle of 27° were presented to investigate the effect of inclination on the flow field. Mean velocities approach self-preservation in both the converging region and the combining region. Velocity fluctuations and Reynolds shear stress approach self-preservation in the combining region only. The spreads of the jet and the square of the decay of maximum mean velocity increase linearly as the distance from the nozzle exit increases.

The exit geometry has a direct effect on the profile and nature of the inlet jet. An experimental investigation reports the centerline evolutions of turbulent properties in nine air jets issuing from differently-shaped nozzles into still air surroundings [XIV]. All nozzles of the investigations have nominally identical opening areas, and their aspect ratio varies from 1 (circle) to 2.5 (isosceles triangle). Measurements were made at the Reynolds number of approximately 15. 10^3. When the Reynolds number is greater than 2000, jets become turbulent as experimentally indicated in reference [XI]. It is found that the loss of axisymmetry of the initial jet configuration generally results from an increase in the near-field decay rate of the mean velocity and turbulence intensity. It is also shown that a change of shape of the nozzle exit does not affect the asymptotic decay rate of the centerline velocity in the far-field.

A numerical investigation of two parallel turbulent plane jets was performed by N. Hnaien et al [IX]. Several turbulence models are compared to finally adopt the standard k-ε in all computations. An improvement in the velocity profile prediction compared to that of Anderson and Spall [II] is obtained. Many important results are found. For a velocity ratio r=1, the increase in the nozzle spacing s is accompanied by a displacement of the merge and combined points further downstream in the longitudinal direction. This movement follows a linear function. For a velocity ratio r>1, the merge and the combined points are no longer located on the symmetry axis (y=0). Increasing the velocity ratio moves these points further upstream in the longitudinal direction while deflecting toward the strong jet in the transverse direction. Nozzle spacing effect on the axial location of the merge and combined point decreases by increasing the velocity ratio while this effect on the transverse positions increases. Numerical results can be extended to more than two parallel jets, like the numerical study of Pandey et al [XVII], who examined the interaction of four parallel jets.

More recently, the effects of the Reynolds number on twin circular jets for small space ratio 1.2 are experimentally studied [XXI], where three Reynolds numbers are considered: Re = 16300, 34400, and 49200. Numerical simulations indicate that the interaction between the jets causes bending of the inner shear layers towards the

symmetry plane. In the far-field after X/D = 5, the jet behaves like a single jet, and a sudden increase of pressure was evident at the exit of the jet along the centerline for all Reynolds numbers. On the other hand, a sharp decrease and increase of mean velocity are noticed at the near field for lateral direction and this peak value increases as Re increases.

Many experimental studies were performed to investigate the effects of nozzle spacing between twin rectangular jets [XV, XVI, III, V]. The instantaneous and mean flow, turbulence intensities, and Reynolds shear stress were studied [XV]. It was observed that changing the nozzle spacing ratio resulted in a linear increase in the locations of the merging and the combined points, with the latter being more affected than the former. It was observed that in the combined region both the decay and spread rates decrease compared to their counterparts in the converging and the merging regions. Hence, within a specific distance from the nozzle, larger spacing ratios resulted in higher decay and spread rates. In the converging region, with an increase in nozzle spacing ratio, the inner shear layers of the jets were able to develop more freely, resulting in a similar spatial distribution of Reynolds shear stress between the inner and the outer shear layers.

To understand Supersonic flows with twin free jet flow at various Mach numbers, a numerical study is carried out by Pandey et al [XVIII]. The purpose was to understand the fluid dynamics and variation of flow properties such as velocity, pressure, and turbulence for various Mach numbers, pressure ratio, and spacing between the two jets. The results show that the jet flow field and the merging process of the two jets vary with the spacing between the two jets. The width of the twin jets flow spreads linearly downstream and grows with dimensionless spacing.

Twin jets configurations can be extended to the simulation of the noise generated from a supersonic flow [VIII]. The computed noise spectra are compared with the experimental data. Numerical simulation with a high-order finite difference solver shows that the dominant and first harmonic modes in the twin jets are amplified dramatically compared with the single jet. Results from Large Eddy Simulations are used to investigate the interaction details of twin rectangular jets of aspect ratio 2:1 over a wide spectrum of operating conditions covering all flight regimes [X]. Wavelet analysis coupled with signal coherence analysis revealed the out-of-phase behavior of twin jets at peak screeching conditions that led to tone attenuation and noise reduction.

The effect of surface curvature is investigated by placing a cylindrical convex body between two jets [VII]. Velocity and turbulence intensity profiles are compared with the previous twin jet measurements. It is observed that a convex surface deflects the jets towards the symmetry axis more strongly and accelerates the flow development procedure.

Through all these works we have just mentioned that very few studies focused on the investigation of flow characteristics when an obstacle is placed between the two jets, because of the difficulty of accurately predicting the interaction of flow structures.

This study aims to investigate numerically the effect of placing a triangular solid object between two parallel jets at the nozzles exit. The Fluent software was used to solve the governing dynamic equations, due to its efficiency to provide reasonable solutions in many earlier studies [XXVII, IV, I]. By varying Reynolds number, flow field and turbulent velocities are examined and compared with the configuration without obstacle.

II. Geometrical configuration

The studied geometrical configurations are shown in Figure 1. We consider two parallel turbulent jets where the distance between nozzles' centerline is S and nozzles' width is d (S/d=6). Dimensions adopted in the transverse and longitudinal directions are respectively 100d and 200d. Configurations are denoted by A and B. They are shown in Fig .1. Configuration B is characterized by the placement of a triangular object between nozzles compared to configuration A.

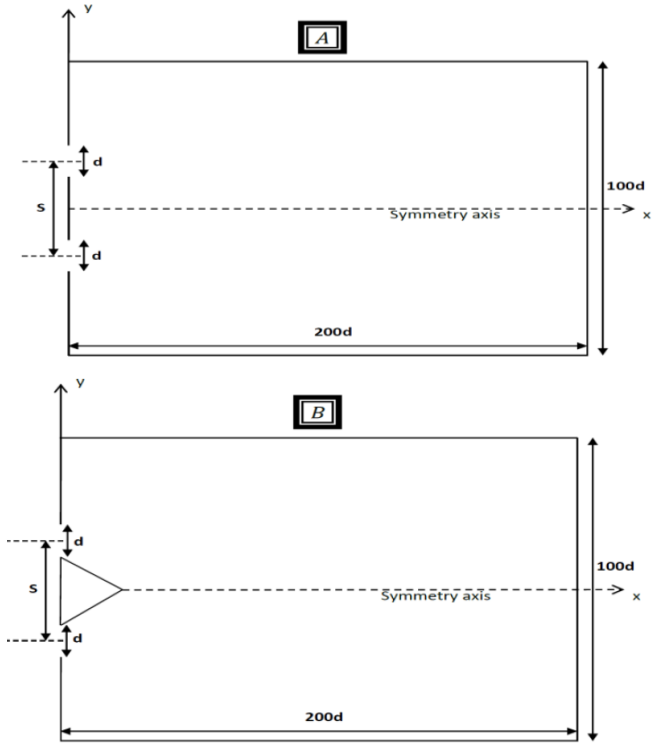

Fig 1. Geometrical configurations

The working fluid is air, which is assumed to be incompressible and with constant thermo-physical properties. Reynolds number based on the inlet velocity and the nozzle width varied from $Re=2.10^3$ to $Re=10^4$. Turbulence intensity distribution at the nozzles exit section is uniform (I_0=3%).

III. Governing equations and boundary conditions

The governing equations for turbulent flow are described mathematically by the Reynolds averaged Navier-Stokes equations (RANS). The flow is assumed to be steady, two dimensional and fully developed at the exit of the nozzles. Turbulence intensity at the exit of the nozzles is fixed to 3%. The RANS equations can be written as follows:

$$\frac{\partial U_i}{\partial X_i} = 0, \tag{1}$$

$$\frac{\partial (U_i U_j)}{\partial X_j} = -\frac{1}{\rho}\frac{\partial P}{\partial X_i} + \frac{\partial}{\partial X_j}\left[\nu \frac{\partial U_i}{\partial X_j} - \overline{u_i u_j}\right], \tag{2}$$

Where turbulence stress is approximated as:

$$\overline{u_i u_j} = \frac{2}{3}\delta_{ij} K - \nu_t \left(\frac{\partial U_i}{\partial X_j} + \frac{\partial U_j}{\partial X_i}\right), \tag{3}$$

Where the Kronecker delta is given by δ_{ij} =1 if (i=j) and δ_{ij} =0 if (i ≠ j), and the turbulence viscosity is defined as:

$$\nu_t = C_\mu \frac{K^2}{\varepsilon}, \tag{4}$$

Turbulence is modeled by three different models: the standard k-ε model, the Realizable model [XX], based on the k-ε model derived from the stationary Reynolds average Navier-Stokes equations, and the RNG k-ε model.

The standard k- ε model

For this model, the turbulence kinetic energy K and its rate of dissipation ε are written respectively as follows:

$$\frac{\partial (\rho U_i K)}{\partial X_i} = \frac{\partial}{\partial X_i}\left(\mu + \frac{\mu_t}{\sigma_K}\frac{\partial K}{\partial X_i}\right) + P_K - \rho\varepsilon, \tag{5}$$

$$\frac{\partial (\rho U_i \varepsilon)}{\partial X_i} = \frac{\partial}{\partial X_i}\left(\mu + \frac{\mu_t}{\sigma_\varepsilon}\frac{\partial \varepsilon}{\partial X_i}\right) + C_{\varepsilon 1}\frac{\varepsilon}{K}P_K - C_{\varepsilon 2}\frac{\varepsilon^2}{K}, \tag{6}$$

Wherein:

$$P_K = \overline{u_i u_j}\left(\frac{\partial U_i}{\partial X_j}\right). \tag{7}$$

The constants of this model are indicated in Table 1.

Table 1. Constants of the standard k-ε model

C_μ	$C_{\varepsilon 1}$	$C_{\varepsilon 2}$	σ_k	σ_ε
0.09	1.44	1.92	1	1.3

The Realizable k- ε model

The Realizable model is an eddy-viscosity model similar to the standard k-ε model, which performs better results than the standard k-ε model when flow separation and recirculation occur.

$$\frac{\partial(\rho U_i K)}{\partial X_i} = \frac{\partial}{\partial X_i}\left(\mu + \frac{\mu_t}{\sigma_K}\frac{\partial K}{\partial X_i}\right) + P_K - \rho\varepsilon, \tag{8}$$

$$\frac{\partial(\rho U_i \varepsilon)}{\partial X_i} = \frac{\partial}{\partial X_i}\left(\mu + \frac{\mu_t}{\sigma_\varepsilon}\frac{\partial \varepsilon}{\partial X_i}\right) + C_{\varepsilon 1}\frac{\varepsilon}{K}P_K - \rho C_{\varepsilon 2}\frac{\varepsilon^2}{K + \sqrt{\nu\varepsilon}}\,. \tag{9}$$

The analytical derivation results in a model with constants that are different from those employed in the standard k- ε model, where P_k is the sheer production of turbulence kinetic energy.

$$C_\mu = \frac{1}{A_0 + A_s U^* \frac{K}{\varepsilon}}\,, \tag{10}$$

$$A_s = \sqrt{6}cos\emptyset\,, \tag{11}$$

with:

$$\emptyset = \frac{1}{3}cos^{-1}\left(\sqrt{6}W\right), \tag{12}$$

$$W = S_{ij}S_{jk}S_{ki}/\tilde{S}\,. \tag{13}$$

and the strain tensor is defined as:

$$S_{ij} = \frac{1}{2}\left(\frac{\partial U_i}{\partial X_j} + \frac{\partial U_j}{\partial X_i}\right), \tag{14}$$

$$\tilde{S} = \sqrt{S_{ij}S_{ji}}\,. \tag{15}$$

$$U^* = \sqrt{S_{ij}S_{jk} + \widetilde{\Omega}_{ij}\widetilde{\Omega}_{ij}}\,, \tag{16}$$

$$\widetilde{\Omega}_{ij} = \Omega_{ij} - 2\epsilon_{ij}\omega_k\,, \tag{17}$$

$$\Omega_{ij} = \overline{\Omega_{ij}} - \epsilon_{ij}\omega_k\,. \tag{18}$$

Where ω_k is the angular velocity and $\overline{\Omega_{ij}}$ is the rotation coefficient tensor. The constants of this model are presented in Table 2.

Table 2. Constants of the Realizable k-ε model

A_0	$C_{\varepsilon 1}$	$C_{\varepsilon 2}$	σ_k	σ_ε
4.04	1.42	1.68	1	1.2

The RNG k-ε model

The RNG model is an eddy-viscosity model similar to the standard k-ε model but incorporates near-wall turbulence anisotropy and non-local pressure-strain effects. It is a general low-Reynolds number turbulence model that is valid all the way up to solid walls and therefore does not need to make use of wall functions.

$$\frac{\partial(\rho U_i K)}{\partial X_i} = \frac{\partial}{\partial X_i}\left(\mu + \frac{\mu_t}{\sigma_K}\frac{\partial K}{\partial X_i}\right) + P_K - \rho\varepsilon, \tag{19}$$

$$\frac{\partial(\rho U_i \varepsilon)}{\partial X_i} = \frac{\partial}{\partial X_i}\left(\mu + \frac{\mu_t}{\sigma_\varepsilon}\frac{\partial \varepsilon}{\partial X_i}\right) + C_{\varepsilon 1}\frac{\varepsilon}{K}P_K - C_{\varepsilon 2}\frac{\rho\varepsilon^2}{K} - R_\varepsilon\,, \tag{20}$$

R_ε is an additional term related to mean strain and turbulence quantities as:

$$R_\varepsilon = \frac{C_\mu \rho \eta^3 (1 - \frac{\eta}{\eta_0})}{1 + \beta'\eta^3}\frac{\varepsilon^2}{K}\,, \tag{21}$$

$$\eta = \sqrt{2S_{ij}S_{ij}}\,\frac{K}{\varepsilon}. \tag{22}$$

The constants of this model are presented in Table 3.

Table 3. Constants of the RNG k-ε model

C_μ	$C_{\varepsilon 1}$	$C_{\varepsilon 2}$	η_0	β'
0.0845	1.42	1.68	4.38	0.012

The boundary conditions

The boundary conditions for the considered problem can be expressed as:

- The velocity at the exit of the nozzles is: $U=U_{in}$ and $V_{in}=0$.
- Turbulent kinetic energy and its dissipation rate at the exit of the nozzles are respectively: $K_{in}=1.5(U_{in}I_0)^2$ and $\varepsilon_{in}=K_{in}^{1.5}/\ell$. ℓ: is a turbulent length scale (ℓ=d/10 m) and I_0 is the inlet turbulent intensity.
- At the gap of the outlet, gradients of all variables in the y-direction are set to zero.
- The velocity boundary conditions are fixed to zero over the solid walls.
- Symmetry condition is applied on the horizontal axis between nozzles.

IV. Numerical methods

The governing equations are discretized using finite volumes schemes and the solver is the commercial CFD code FLUENT 16.0. The velocity components are calculated at a staggered grid while the scalar variables are calculated at the main grid (not staggered). For coupling of mass and momentum equations, the SIMPLE algorithm is used [XIX]. The Green-Gauss cell-based scheme is used for gradient discretization. Second-order upwind central differencing is used for flow terms, while first-order upwind central differencing is used for turbulent kinetic energy and turbulent dissipation rate. The convergence criterion was taken 10^{-4} for the normalized residual of each equation. We have used relaxation factors of 0.7 for velocities, 0.8 for turbulent quantities, and 0.3 for pressure.

V. Results and discussion

We Consider two plan parallel jets (S/d=6), where the Reynolds number varied from 2.10^3 to 10^4. When the Reynolds number is greater than 2000, jets become turbulent as experimentally indicated in reference [XI]. The merge point is determined by the stagnation point where the mean velocity is zero on the symmetry axis.

Validation and grid independence

To validate the mathematical model and numerical methods, it has been tested with the experimental results of Anderson and Spall [II].

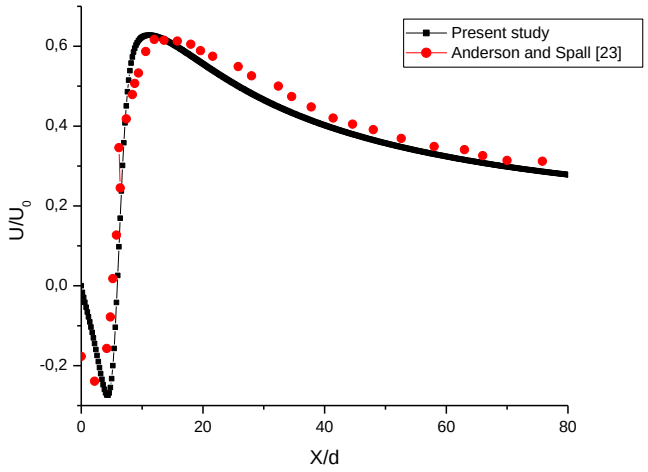

Fig 2. Axial mean velocity distribution along the symmetry axis for S/d=9

The configuration of Anderson and Spall is like configuration **A** with a nozzles spacing (S/d =9). Reynolds number was taken equal to 6000 and turbulent intensity at the outlet of the nozzles was 3.6%. Numerical simulations are obtained with non-uniform meshes of different grid sizes: 600×336, 480×252, and 450×168. Our numerical results show a good agreement with the experimental data as indicated in Figure 2.

The velocity field

The mean axial velocity distribution at the symmetry axis is indicated in Figure 3 for different Reynolds numbers. Since the velocity ratio is one (the same exit velocity for the two nozzles), the axial location of merge and combined points occurs always in the symmetry axis (y=0) as mentioned by Lin and Sheu [XII], and by Anderson and spall [II].

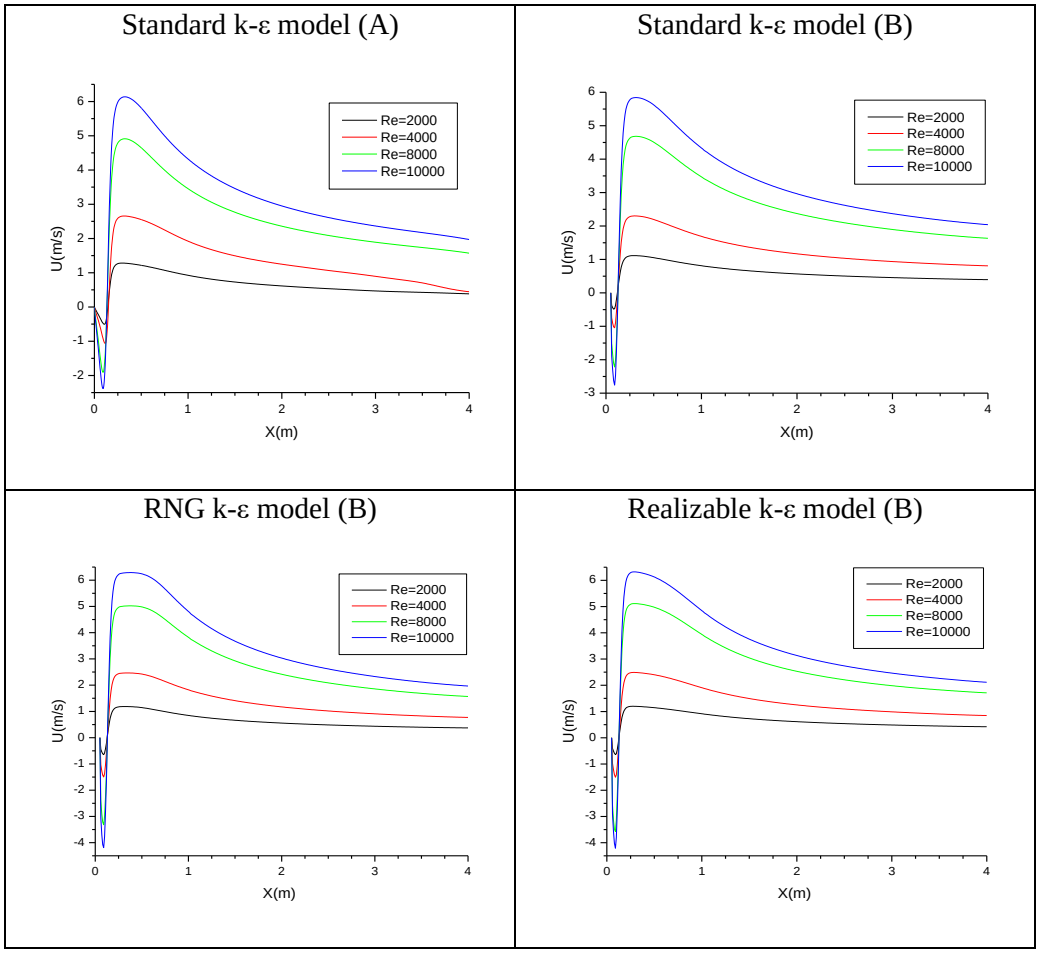

Fig 3. Axial mean velocity distribution along the symmetry axis for different turbulence models

It is observed from Figure 3 that mean axial velocity increases rapidly in the downstream up to X = 0.125m for all Reynolds numbers. The maximum velocity attained in the centerline is higher as Re increases. Mean velocity starts decaying in the further downstream where it resembles the properties of single jet. Negative values of the axial velocity are found in this region, which indicates the existence of a small recirculating zone.

For a given turbulence intensity (I_0=3%), the velocities and their gradients decay along the *x*-axis, due to the effect of entrainment in the shear layer. At the same time, the width of the jet was found to increase with the Reynolds number. Negative values of the velocity are encountered between the nozzle exit and the merging point where a small recirculation region appears.

Merge and combined points

The converging zone is located between the nozzle exit and the point where the inner shear layers of the jets merge. The location where the velocity at the symmetry plane reaches its maximum is called the combined point and denotes that the merging region ends and the combined region begins [XXII, XXV]. The combined zone is downstream of the combined point where the two jets begin to resemble a self-similar single jet. A schematic view of the different regions of dual jets is indicated in Figure 4 [XXI].

Merge and combined point axial locations for configuration B are respectively illustrated in Table 4 and Table 5.

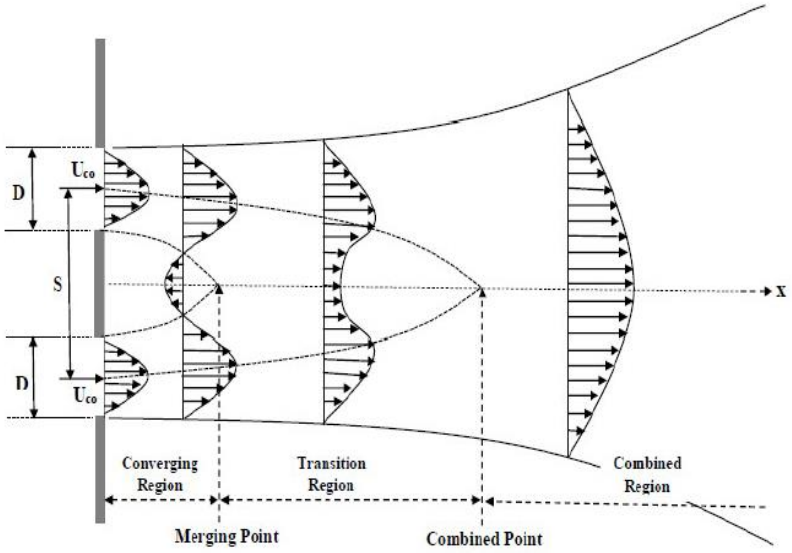

Fig 4. Dual jets flow structure.

Table 4. Merge point locations for the configuration B

	X_{MP}(m) for standard	X_{MP}(m) for Realizable	X_{MP}(m) for RNG
Re=2000	0.119	0.127	0.127
Re=4000	0.123	0.129	0.130
Re=8000	0.125	0.128	0.134
Re=10000	0.125	0.129	0.131

Table 5. Combined point locations for the configuration B

	X_{CP} (m) for Standard	X_{CP} (m) for Realizable	X_{CP} (m) for RNG
Re=2000	0.30	0.27	0.32
Re=4000	0.30	0.29	0.35
Re=8000	0.31	0.30	0.38
Re=10000	0.31	0.29	0.38

We can see that the combined point axial position generally increases with the Reynolds number for all turbulence models. We can see also that compared to the standard k-ε model, the Realizable k-ε model underestimates the location of the combined point, however, the RNG k-ε model overestimates it.

Merge and combined point locations for configuration **A** are indicated in Table 6.

Table 6. Merge and combined point locations for the configuration A

	X_{MP}(m)	X_{CP}(m)
Re=2000	0.144	0.295
Re=4000	0.150	0.315
Re=8000	0.133	0.325
Re=10000	0.133	0.325

We conclude by comparison between Table 6 and the two last tables, that for configuration **B**, the merge point locations are pushed downstream of the flow for all Reynolds numbers. Combined point locations are also affected by the placement of the triangular object between nozzles.

Turbulent kinetic energy

The mean kinetic energy distribution along the symmetry axis for the two configurations is shown in Figure 5. For configuration **A**, turbulent kinetic energy increases fast until it reaches the maximum at X/d = 7 approximately. This means that kinetic energy increases in the near field and dissipates slowly in the far field which implies that energy transfer is greater for higher Reynolds numbers.

For configuration B, a fast increase of turbulent kinetic energy is shown until it reaches the maximum at X/d = 6 approximately. For the same Reynolds number, the maximum of TKE for configuration **B** is lower than the maximum detected for configuration A. The far-field of TKE is also affected by showing the existence of a second peak at X=1 m. The values of this peak increase with Reynolds numbers.

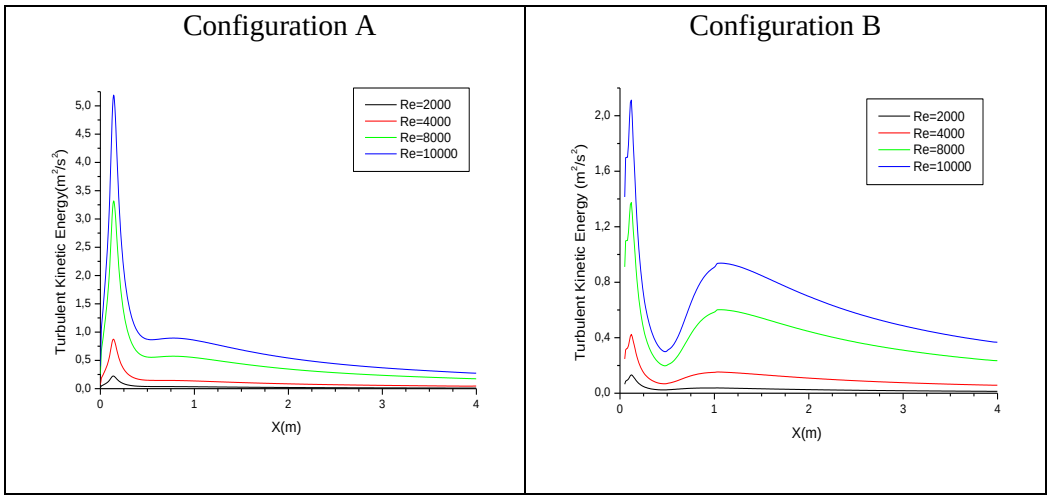

Fig 5. Turbulent kinetic energy profiles at the symmetry axis.

Figure 6 shows turbulent kinetic energy profiles for the three chosen turbulence models at Re=2000. We conclude that the three models show the same behaviors of turbulent kinetic energy at the symmetry axis. However, the peak values detected by the Realizable k-ε model are higher than the peak values detected by the RNG k-ε model and by the Standard k-ε model. This is due to the fact that the Realizable k-ε model overestimates the velocity field, especially for high Reynolds numbers.

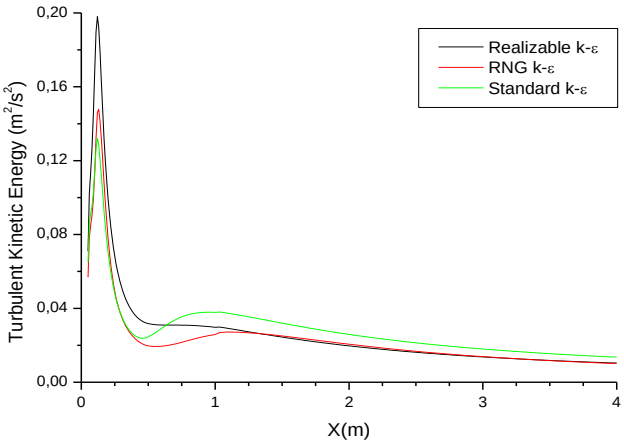

Fig 6. Turbulent kinetic energy profiles at the symmetry axis for Re=2000.

VI. Conclusion

In the present study, we have investigated numerically the effect of placing a triangular object between nozzles in dual turbulent jets. Three turbulence k-ε models are used to predict flow characteristics and turbulent quantities: the Standard k-ε model, the Realizable k-ε model, and the RNG k-ε model. The CFD Fluent 16.0 code is used for the resolution of the transport equations. The numerical method is

validated by the experimental results available. The Reynolds number at the nozzles exit was varied from: $Re=2.10^3$ to $Re=10^4$. For a fixed nozzle spacing (S/d=6), and a fixed inlet intensity (I_0=3%), two configurations denoted by A and B are tested. Configuration B differs from configuration A by the placement of a triangular object between nozzles. The numerical simulation shows that axial locations of merge and combined points are affected by the placement of the triangular object for all Reynolds numbers. The merge point axial position is pushed downstream of the flow and the corresponding axial velocity at the combined point for configuration B is reduced compared to configuration A. The turbulent kinetic energy field is also affected, either in the near field or in the far-field for all Reynolds numbers. We have concluded also that the Realizable k-ε model overestimates velocity and turbulent kinetic energy fields compared to the other models.

References

I. Abbasalizadeh M., Jafarmadar S. and Shirvani H., "The effects of pressure difference in nozzle's two phase flow on the quality of exhaust mixture", International Journal of Engineering Transactions B: Applications, vol. 26, no. 5, pp: 553-562, 2013.

II. Anderson E. A. and Spall R. E., "Experimental and numerical investigation of two-dimensional parallel jets", Transactions of ASME, Journal of Fluids Engineering, vol. 123, no. 2, pp: 401-406, 2001.

III. Azim M. A., "Characteristics of twin axisymmetric free jets", Proceedings of the international Conference on Mechanical Engineering, Bangladesh, 2009.

IV. Boussoufi M., Sabeur-Bendehina A., El Ganaoui M., Morsli S. and Ouadha A., Numerical simulation of the flow field analysis in the mixing twin jets, Energy Procedia, vol. 139, pp: 161-166, 2017.

V. Elbanna H., Sabbagh J. A. and Rashed M. I. I, "Interception of two equal turbulent jets", AIAA Journal, vol. 23, no. 7, pp: 985-986, 1985.

VI. Elbanna H., Gahin S. and Rashed M. I. I., "Investigation of two plane parallel jets", AIAA Journal, vol. 21, no. 7, 986-991, 1983.

VII. Erdem D. and Ath V., "Interaction of two parallel rectangular jets", 23rd International Congress of Aeronautical Sciences, Canada, 2002.

VIII. Gao J., Xu X. and Li X., "Numerical simulation of supersonic twin-jet noise with high-order finite difference scheme", AIAA Journal, vol. 56, no. 1, pp: 290-300, 2018.

IX. Hnaien N., Marzouk Khairallah S., Ben Aissia H and Jay J, "Numerical study of interaction of two plane parallel jets", International Journal of Engineering TRANSACTIONS A: Basics, vol. 29, no. 10, pp: 1421-1430, 2016.

X. Karnam A., Baier F., Gutmark E. J., Jeun J., Wu G. J. and Lele S. K., "An investigation into flow field interactions between twin supersonic rectangular jets", AIAA Scitech forum, January 2021.

XI. Kwon S. J. and Seo I. W., "Reynolds number effects on the behavior of a non-buoyant round jet", Experiments in Fluids, vol. 38, no. 6, pp: 801-812, 2005.

XII. Lin Y. F. and Sheu M. J., "Interaction of parallel turbulent plane jets", AIAA Journal, vol. 29, no. 9, pp: 1372-1373, 1991.

XIII. Lin Y. F. and Sheu M. J., "Investigation of two plane parallel unventilated jets", Experiments in Fluids, vol. 10, no. 1, pp: 17-22, 1990.

XIV. Mi J. and Nathan G. J., "Statistical properties of turbulent free jets issuing from nine differently-shaped nozzles", Flow, Turbulence and Combustion, vol. 84, pp: 583-606, 2010.

XV. Naseri Oskouie R., Tachie M. F. and Wang B. C., "Effect of nozzle spacing on turbulent interaction of low-aspect-ratio twin rectangular jets", Flow, Turbulence and Combustion, vol. 103, no. 2, pp: 323, 2019.

XVI. Nasr A. and Lai J. C. S., "Two parallel plane jets: mean flow and effects of acoustic excitation", Experiments in Fluids, vol. 22, no. 3, pp: 251-260, 1997.

XVII. Pandey K. M. and Kumar V., "CFD analysis of four jet flow at Mach 1.74 with Fluent software", International Journal of Environmental Science and Development, vol. 1, no. 5, pp: 423-428, 2010.

XVIII. Pandey K. M., Kumar V. and Srivastava P., "CFD analysis of twin jet supersonic flow with Fluent software", Current Trends in Technology and Sciences, vol. 1, no. 2, pp: 84-91, 2012.

XIX. Patankar S. V., Numerical heat transfer and fluid flow, Mac Graw Hill, New York, 1980.

XX. Shih T. H., Liou W. W., Shabbir A., Yang Z. and Zhu J., A new k-ε eddy viscosity model for high Reynolds number turbulent flows, Computer and Fluids, vol. 24, no. 3, pp: 227-238, 1995.

XXI. Sourav S., Hossain Rifat A. and Taher Ali M. A., "Effects of Reynolds number on twin circular jets at a small space ratio", International Journal of Research and Scientific Innovation, vol. 7, no. 8, pp: 248-252, 2020.

XXII. Spall R. E., Numerical study of buoyant plane parallel jets, Journal of Heat Transfer, vol. 124, no. 6, pp: 1210-1212, 2002.

XXIII. Tanaka E., "Experiments on the combined flow of dual jet: the interference of two-dimensional parallel jets", Bulletin JSME, vol. 17, no. 109, pp: 920-927, 1974.

XXIV. Tanaka E., "The interference of two dimensional parallel jets", Bulletin JSME, vol. 13, no. 56, pp: 272-280, 1970.

XXV. Tenchine D. and Moro J. P., "Experimental and numerical study of coaxial jets", Proceedings of the 8th Int topical meeting on nuclear reactor thermal-hydraulics, Japan, vol. 3, pp: 1381-1387, 1997.

XXVI. Wang C. S., Lin Y. F. and Sheu M. J., "Measurements of turbulent inclined plane dual jets", Experiments in Fluids, vol. 16, no. 1, pp: 27-35, 1993.

XXVII. Zheng X., Jian X., Wei J. and Wenzheng D., "Numerical and experimental investigation of near-field mixing in parallel dual round jets", International Journal of Aerospace Engineering, vol. 1, pp: 1-12, 2016.